Electrical characterization of deep levels created by bombarding nitrogen-doped 4H-SiC with alpha-particle irradiation

Ezekiel Omotoso[1,2,a)], Walter E. Meyer[1], F. Danie Auret[1], Alexander T. Paradzah[1] and Matshisa J. Legodi[1]

[1] *Department of Physics, University of Pretoria, Private Bag X20, Hatfield 0028, South Africa*
[2] *Departments of Physics, Obafemi Awolowo University, Ile-Ife, 220005, Nigeria*
[a)] *Corresponding and presenting author's e-mail address and contact number: ezekiel.omotoso@up.ac.za; wmeyer@up.ac.za +274842911287*

ABSTRACT

Deep-level transient spectroscopy (DLTS) and Laplace-DLTS were used to investigate the effect of alpha-particle irradiation on the electrical properties of nitrogen-doped 4H-SiC. The samples were bombarded with alpha-particles at room temperature (300 K) using an americium-241 (^{241}Am) radionuclide source. DLTS revealed the presence of four deep levels in the as-grown samples, $E_{0.09}$, $E_{0.11}$, $E_{0.16}$ and $E_{0.65}$. After irradiation with a fluence of 4.1 × 10^{10} alpha-particles-cm^{-2}, DLTS measurements indicated the presence of two new deep levels, $E_{0.39}$ and $E_{0.62}$ with energy level, E_C – 0.39 eV and E_C –0.62 eV, with an apparent capture cross sections of 2×10^{-16} and 2×10^{-14} cm^2, respectively. Furthermore, irradiation with fluence of 8.9×10^{10} alpha-particles-cm^{-2} resulted in disappearance of shallow defects due to a lowering of the Fermi level. These defects re-appeared after annealing at 300℃ for 20 minutes. Defects, $E_{0.39}$ and $E_{0.42}$ with close emission rates were attributed to silicon or carbon vacancy and could only be separated by using high resolution Laplace-DLTS. The DLTS peaks at E_C – (0.55-0.70) eV (known as Z_1/Z_2) were attributed to an isolated carbon vacancy (V_C).

Keywords: DLTS, 4H-SiC, alpha-particle irradiation, annealing, Schottky barrier diode

1. Introduction

The importance of deep level defects that act as charge carrier traps in semiconductor industry and applications of semiconductor devices cannot be over-emphasized [1, 2]. The deep level defects (both hole and electron traps) are being formed during the growth of the semiconductor, processing during fabrication of the electronic device (e.g. electron beam and sputtering deposition) and operation in radiation harsh environment. Deep levels can be introduced intentionally into electronic devices and can be beneficiary or detrimental. For detrimental defects, it is important to find methods to remove these defects. Some of the defects anneal out at room or elevated temperatures while some emanate at certain annealing temperature. The signatures of a deep level (i.e. its activation energy in the band gap and

apparent capture cross section) can be determined from temperature depended deep level transient spectroscopy (DLTS) and Laplace DLTS measurements on Schottky barrier diodes (SBDs). Effects of radiation and annealing temperature on semiconductors are technologically important for radiation sensing applications as well as manufacturing processes and high temperature and high power applications [3].

SiC is a promising semiconductor with a wide bandgap of 3.26 eV [4]. Because of its wide bandgap, SiC is a suitable substrate for developing devices that are capable of operating at high temperature as well as in harsh radiation fields [5, 6], such as space, accelerator facilities and nuclear power plants [7-9]. The electrical and thermal properties of SiC also make it suitable electronic devices operating at high power, high temperature and high frequency [10]. Furthermore, SiC is a key material for the next generation of photonics [11]. Because of the aforementioned features, SiC is superior to Si in a number of applications.

In this work, the effect of alpha-particle irradiation at high fluences and annealing of 4H-SiC has been investigated by means of current-voltage (*I*-*V*), capacitance-voltage (*C*-*V*), DLTS and Laplace DLTS measurements. The major aim was to determine the effect of irradiating *n*-type 4H-SiC at high fluence and investigate the annealing of these defects.

2. Experimental procedure

The samples used for this work were cut from a nitrogen-doped *n*-type 4H-SiC wafer. The samples were grown on the Si-face of a SiC substrate with a net doping density of 10^{18} cm^{-3} and a resistivity of 0.02 Ω-cm. The epilayer had a doping density of 7.1×10^{15} cm^{-2}. The wafers were supplied by CREE Res. Inc.

The samples were cut into smaller pieces and prepared according to the procedure reported by Omotoso *et al* [12]. Resistive evaporation was employed for the deposition of ohmic and Schottky contacts since it does not introduce defect(s) in measurable quantity. Nickel was used for both contacts. The ohmic contact with a thickness of 3000 Å was deposited at a rate of 0.9 $Å s^{-1}$ onto the highly doped (10^{18} cm^{-3}) back surface of the samples. The samples were annealed in a tube furnace under flowing argon at 950℃ for 10 minutes to form nickel silicides [13] in order to obtain low resistivity ohmic contacts. Before deposition of the Schottky contacts, the samples were degreased as previously reported [12]. Directly after cleaning, the samples were inserted into vacuum chamber where NiAu (20 % Au) Schottky contacts were resistively evaporated through a metal contact mask on Si-face. The diameter

and the thickness of the Ni/Au Schottky barrier diodes (SBDs) were 0.57 mm and 1000 Å respectively, and they were deposited at a rate of 0.5 Ås^{-1} under a vacuum of approximately 3×10^{-5} mbar on Si-face.

The samples were irradiated at room temperature with alpha particles of average energy of 5.4 MeV by placing the samples on a ^{241}Am radio-nuclide foil. The samples were irradiated for 16 hours, measured, and then irradiated for a further 19 hours. The fluence rate from this foil was 7.1×10^{6} alpha-particles $cm^{-2}s^{-1}$. The total fluence received by the SBD after 19 hours was 8.9×10^{11} alpha-particles cm^{-2}. The quality of the Schottky barrier diodes was tested by carrying out current-voltage (*I-V*) and capacitance-voltage (*C-V*) measurements in the dark at room temperature. The *I-V* and *C-V* measurements were carried out by an HP 4140 B pA meter/DC voltage source and an HP 4192A LF Impedance Analyzer, respectively. Conventional DLTS as well as Laplace DLTS were used to characterize the defects present in the as-grown and alpha-particle irradiated material, as well as after annealing in argon ambient at 300℃ for 20 minutes.

3. Results and discussion

3.1. I-V characteristics at room temperature

I-V and *C-V* measurements were performed to test the suitability of the devices for the study. Fig. 1 shows the semi-logarithmic *I-V* characteristics of the Schottky barrier diodes (SBDs) as grown *(i)*, after bombardment with a fluence of 4.1×10^{11} *(ii)* and 8.9×10^{11} cm^{-2} *(iii),* and after annealing at 300℃ for 20 minutes in flowing argon *(iv)*. The effect of irradiation and annealing on the SBDs can be quantified in terms of the ideality factor (n), Schottky barrier height (ϕ_b), saturation current (I_s) and series resistance (R_s), as obtained from the plots in Fig. 1. The ideality factor obtained in *(i)* was 1.12 suggesting that thermionic emission is the dominant current transport mechanism. In *(ii)* and *(iii)*, the ideality factor increased to 1.20 and 1.77, respectively. The increase in ideality factor was attributed to deviation from thermionic emission. This suggests that other current transport mechanisms such as generation recombination could be dominant as well especially at lower voltages. Above 0.7 V, series resistance is dominant in *(iii)*. After the annealing at 300℃, the dominance of series resistance reduced as shown in the plot represented by *(iv)*. Table 1 compares the properties of the diode at aforementioned conditions. The ϕ_b of the contacts were determined from the *I-V* characteristics analysed using the thermionic emission model [14, 15]. The I_s was derived from the straight line intercept of log *I-V* plot at $V = 0$. The

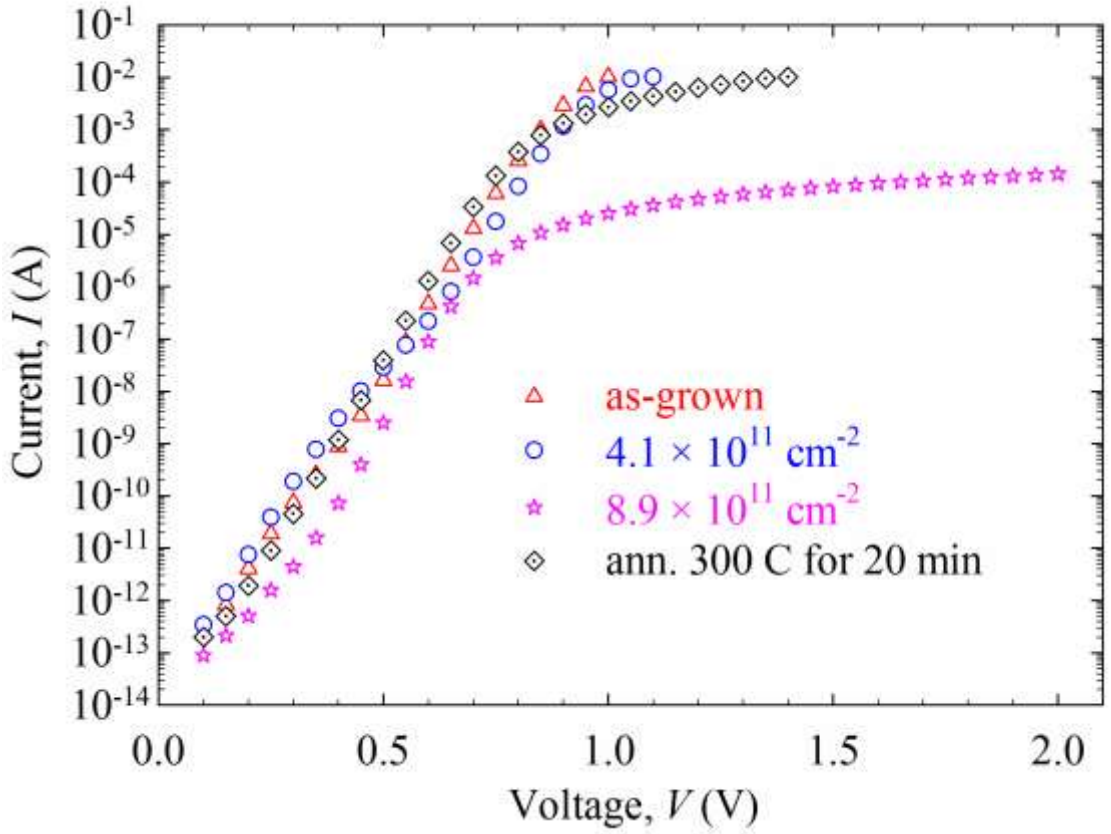

Fig. 1. Forward *I-V* characteristics of 4H-SiC SBD in as-grown *(i)*, irradiated with 5.4 MeV alpha-particles at fluence 4.1×10^{11} *(ii)* 8.9×10^{11} cm^{-2} *(iii)*, and after annealing at 300℃ for 20 minutes in flowing argon *(iv)*, measured at 300 K.

Table 1

Comparison of some electrical parameters of 4H-SiC in as-grown *(i)*, irradiated with 5.4 MeV alpha-particles at fluence 4.1×10^{11} *(ii)* 8.9×10^{11} cm^{-2} *(iii)*, and after annealing at 300℃ for 20 minutes in flowing argon *(iv)*. The parameters estimated from *I-V* and *C-V* characteristics measured at 300 K.

Process	n	I_s (A)	R_s (Ω)	V_{bi}	N_D (cm^{-3})	$\phi_{b,\,I\text{-}V}$ (eV)	$\phi_{b,\,C\text{-}V}$ (eV)
(i)	1.12	2.1×10^{-14}	12	0.93	7.0×10^{15}	1.06	1.21
(ii)	1.20	1.1×10^{-14}	15	2.38	4.6×10^{15}	1.08	2.68
(iii)	1.77	6.9×10^{-15}	13000	18.3	2.9×10^{15}	1.09	18.6
(iv)	1.15	1.9×10^{-15}	48	2.96	4.4×10^{15}	1.13	3.25

fluence and annealing dependency of n, $\phi_{b,\,I\text{-}V}$ and I_s may connected to the movement (or shift) of Fermi level pinning at the surface of SiC, since irradiation-induced defects can create interface states. Fig. 2 shows the plot of C^{-2} (pF^{-2}) as a function of voltage, V (V) for *(i)* to *(iv)* processes as defined earlier, all were measured at 1 MHz frequency with the sample at room temperature. The capacitance increased with decrease in reverse voltage for all conditions, but the capacitance of *(iii)* was the lowest and very distinct from others because of

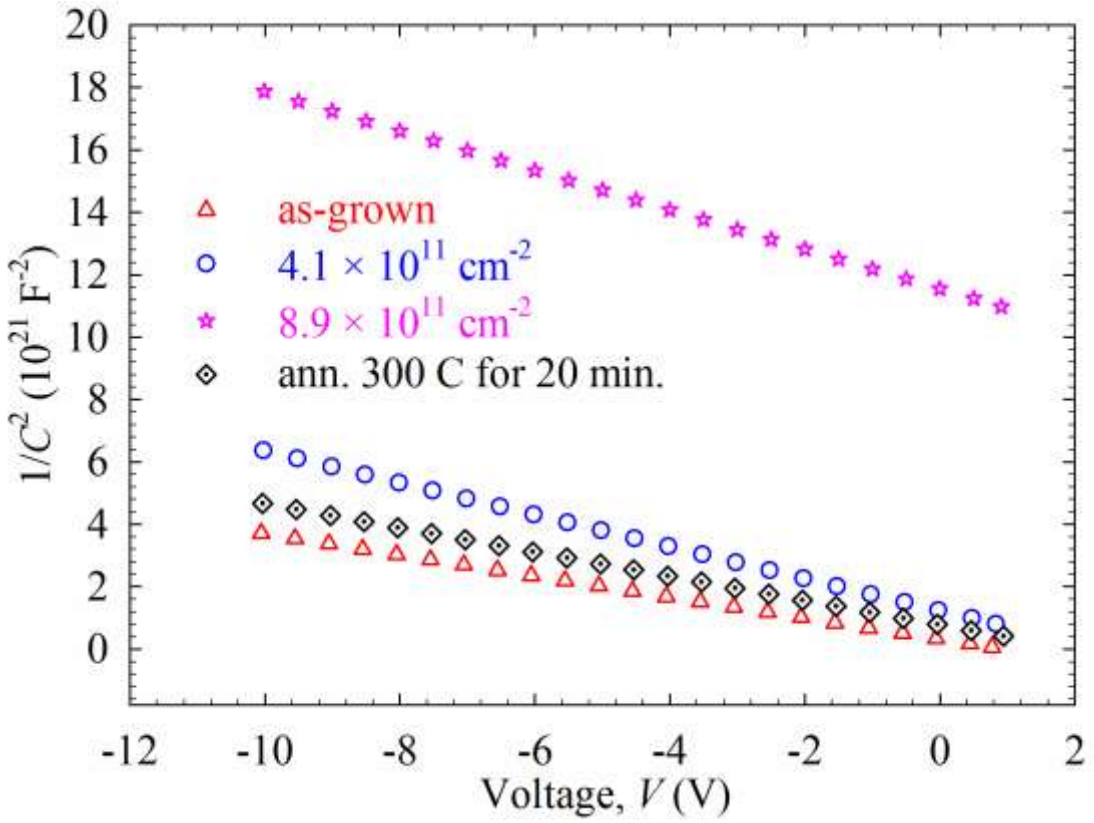

Fig. 2. $1/C^2$ as a function of voltage characteristics of 4H-SiC SBDs in as-grown *(i)*, irradiated with 5.4 MeV alpha-particles at fluence 4.1×10^{11} *(ii)* 8.9×10^{11} cm^{-2} *(iii)*, and after annealing at 300 ℃ for 20 minutes in flowing argon *(iv)*, measured at 300 K.

the position of the Fermi level with respect to the conduction band. A decrease in the capacitance after irradiation was attributed to the reduction of net donor concentration at 4H-SiC interface due to the effect of radiation induced defects. The *C-V* characteristics for the different conditions are also tabulated in Table 1.

3.2. Conventional DLTS analysis

Fig. 3 shows the DLTS spectra for SBD under different conditions. The measurements were obtained over a temperature range 30-380 K, at a quiescent reverse bias of −5.0 V, filling pulse amplitude of 6.0 V, filling pulse width of 1.0 ms and at different rate windows (2.5 to 1000 s^{-1}). The *signatures* of the defects in terms of activation energy, E_n and apparent capture cross section, σ_n were determined from the Arrhenius plot in Fig. 4. The activation energy of each defect was determined from the slope, and the corresponding apparent capture cross section was calculated from the intercept of the Arrhenius plot of log (T^2/e_n) versus *1/T*

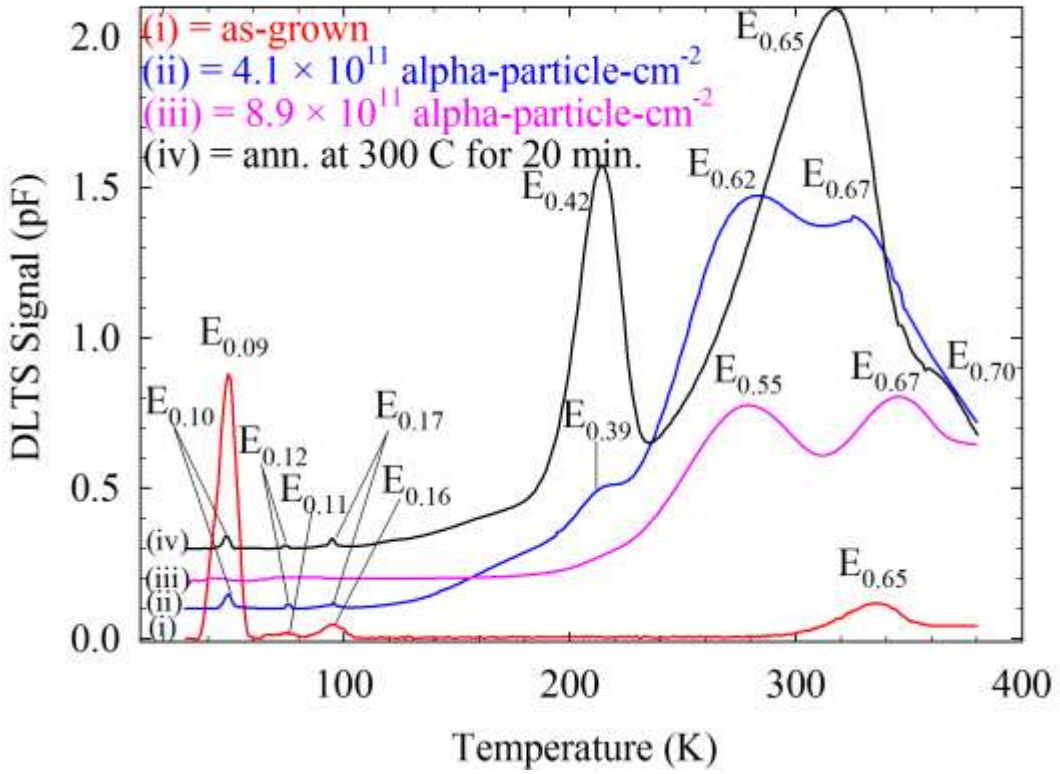

Fig. 3. Conventional DLTS spectra of 4H-SiC showing the present of defects in as-grown *(i)*, irradiated with 5.4 MeV alpha-particles at fluence 4.1×10^{11} *(ii)* 8.9×10^{11} cm^{-2} *(iii)*, and after annealing at 300℃ for 20 minutes in flowing argon *(iv)*. In curve *(i)*, the spectrum was scaled up by factor of 5 from 55 to 380 K. The rate window is 200 s^{-1}.

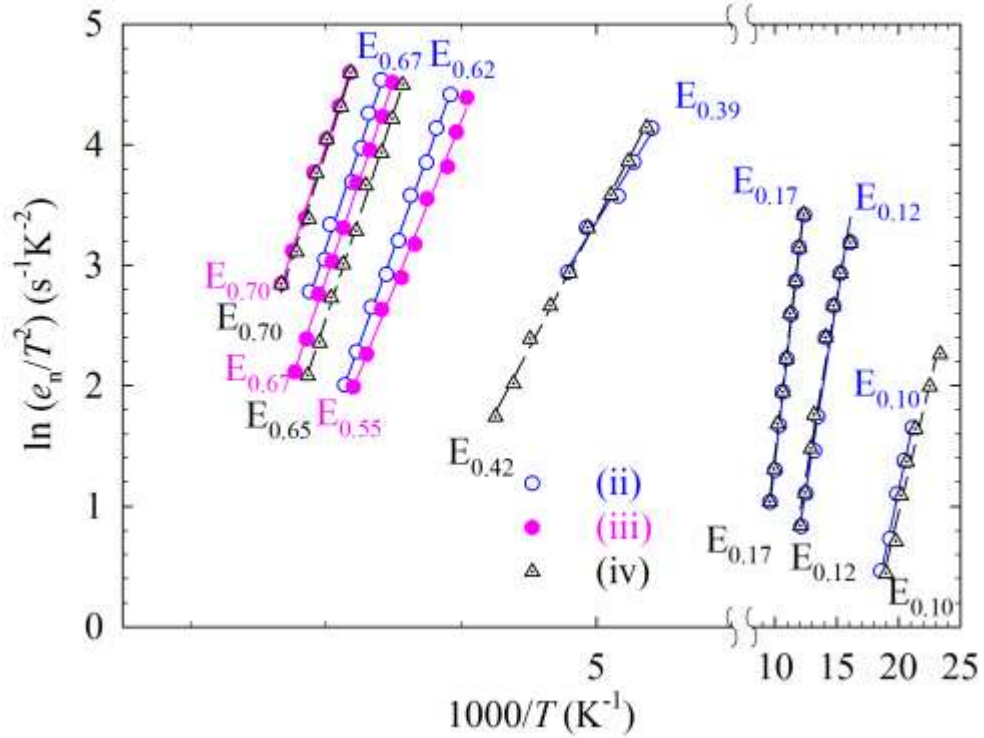

Fig. 4. Arrhenius plots of 4H-SiC SBD for irradiated with 5.4 MeV alpha-particles at fluence 4.1×10^{11} *(ii)* 8.9×10^{11} cm^{-2} *(iii)*, and after annealing at 300℃ for 20 minutes in flowing argon *(iv)*.

as reported by Auret *et al* [16]. The attributes of all the electron traps in *(i)* to *(iv)* are tabulated in Table 2.

Table 2
Electronic properties of defects detected in 4H-SiC SBD by DLTS in as-grown *(i)*, irradiated with 5.4 MeV alpha-particles at fluence 4.1×10^{11} *(ii)* 8.9×10^{11} cm^{-2} *(iii)*, and after annealing at 300 ℃ for 20 minutes in flowing argon *(iv)*, and L-DLTS after process after *(iv)*.

Process	Defect label	E_T [eV]	σ_a [cm^2]	Defect ID	Refs.
(i)	$E_{0.09}$	$E_C - 0.09$	8×10^{-15}	N	[18]
	$E_{0.11}$	$E_C - 0.11$	2×10^{-16}	Ti	[25]
	$E_{0.16}$	$E_C - 0.16$	1×10^{-15}	Ti	[20]
	$E_{0.65}$	$E_C - 0.65$	4×10^{-15}	V_C (Z_1/Z_2)	[21, 23]
(ii)	$E_{0.10}$	$E_C - 0.10$	8×10^{-14}	N	[18]
	$E_{0.12}$	$E_C - 0.12$	2×10^{-15}	Ti	[25]
	$E_{0.17}$	$E_C - 0.17$	9×10^{-15}	Ti	[20]
	$E_{0.39}$	$E_C - 0.39$	2×10^{-16}	$V_{C/Si}$	[19]
	$E_{0.62}$	$E_C - 0.62$	2×10^{-14}	V_C (Z_1/Z_2)	[21, 23]
	$E_{0.67}$	$E_C - 0.67$	2×10^{-15}	V_C (Z_1/Z_2)	[21, 23]
(iii)	$E_{0.55}$	$E_C - 0.55$	2×10^{-15}	V_C (Z_1/Z_2)	[20, 22]
	$E_{0.67}$	$E_C - 0.65$	3×10^{-15}	V_C (Z_1/Z_2)	[21, 23]
	$E_{0.70}$	$E_C - 0.70$	1×10^{-15}	V_C (Z_1/Z_2)	[21, 23]
(iv)	$E_{0.10}$	$E_C - 0.10$	9×10^{-15}	N	[18]
	$E_{0.12}$	$E_C - 0.12$	5×10^{-16}	Ti	[25]
	$E_{0.17}$	$E_C - 0.17$	7×10^{-15}	Ti	[20]
	$E_{0.42}$	$E_C - 0.42$	6×10^{-15}	$V_{C/Si}$	[19]
	$E_{0.65}$	$E_C - 0.67$	1×10^{-14}	V_C (Z_1/Z_2)	[21, 23]
	$E_{0.70}$	$E_C - 0.70$	2×10^{-15}	V_C (Z_1/Z_2)	[21, 23]
L-DLTS	$E_{0.39}$	$E_C - 0.39$	5×10^{-15}	$V_{C/Si}$	[19]
	$E_{0.42}$	$E_C - 0.42$	5×10^{-15}	$V_{C/Si}$	[19]
	$E_{0.65}$	$E_C - 0.65$	8×10^{-15}	V_C (Z_1/Z_2)	[21, 23]
	$E_{0.70}$	$E_C - 0.70$	4×10^{-14}	V_C (Z_1/Z_2)	[21, 23]
	$E_{0.76}$	$E_C - 0.74$	1×10^{-14}	?	[19, 24]

Curve *(i)* is the spectrum of the as-grown sample and indicates the presence of four electron traps ($E_{0.09}$, $E_{0.11}$, $E_{0.16}$ and $E_{0.65}$) with energies 0.09, 0.11, 0.16 and 0.65 eV below the conduction band. These defects were associated with the growth of 4H-SiC. The Arrhenius plots of the defects present in as-grown 4H-SiC as well as their attributes have been reported by Omotoso *et al*. [12, 17].

In curve *(ii)*, the amplitude of the shallow defect labelled $E_{0.09}$ was reduced to 12% of its height in the as-grown material. The defects labelled $E_{0.09}$ and $E_{0.10}$ have identical level, and slightly different energy. The $E_{0.09/0.10}$ has been assigned to nitrogen impurities that occupy the cubic site [18]. The defect labelled $E_{0.39}$ with energy, 0.39 eV below the conduction band emanated after the diode received a fluence of 4.1×10^{11} alpha-particle-cm^{-2} from a ^{241}Am source. The level labelled $E_{0.39}$ has been attributed to silicon vacancy (V_{Si}) [19]. The defect $E_{0.65}$ from as-grown was replaced with two defects with energies 0.62 and 0.67 eV and both

displaying broad peaks. From curve *(ii)*, we conclude that ^{241}Am with energy 5.4 MeV introduced new defects into the diode after bombardment with fluence 4.1×10^{11} alpha-particle-cm^{-2}.

Curve *(iii)* was measured after bombardment of the devices with total fluence of 8.9×10^{11} alpha-particle-cm^{-2}. From curve *(iii)*, the disappearance of shallow defects ($E_{0.09/0.10}$, $E_{0.11/0.12}$ and $E_{0.16/0.17}$) occurred. It was as a result of intense damage that lowered the position of Fermi level deeper into the bandgap, below the shallow defect levels. The result is that these defects were never filled by the DLTS filling pulse and therefore remain invisible. Also, the two broad defects observed earlier in *(ii)* remained, displaying activation energies and apparent capture cross sections as 0.55 and 0.67 eV, and 2.4×10^{-15} and 2.9×10^{-15} cm^2, respectively. In addition to those electron traps present in *(iii)*, $E_{0.70}$ with activation energy of 0.70 eV and apparent capture cross section of 1.0×10^{-15} cm^2 appeared above 380 K for rate window plotted, but was only visible at much lower rate windows. We believe that the $E_{0.62}$ and $E_{0.67}$ in curve *(ii)* are due to the same defect as the $E_{0.55}$ and $E_{0.67}$ in curve *(iii)*. The reason for the difference in the observed peak shapes and position difference between the $E_{0.62}$ and $E_{0.55}$ in the two curves may be explained by the field effect. Since the carrier concentration for curve *(iii)* is much lower than that for curve *(ii)*, it follows that the defects measured in curve *(ii)* experience a higher electric field. Due to field enhanced emission, the peaks in curve *(ii)* are therefore expected to move towards the lower temperature. This seems to be true for the $E_{0.67}$ in curves *(ii)* and *(iii)*.

Curve *(iv)* was recorded after annealing the twice irradiated device, in flowing argon at 300℃ for 20 minutes. The shallow defects re-appeared, the $E_{0.42}$ (which has the same attribute with $E_{0.39}$) became distinct and prominent, and also the two distinct defects in *(iii)* ($E_{0.55}$ and $E_{0.65}$) reduced to one prominent defect with electron trap label, $E_{0.67}$ and a defect $E_{0.74}$ as a shoulder at the high-temperature end of the $E_{0.65}$. The re-appearance of the low energy defects is consistent with our explanation for their disappearance in curve *(iii)*: After annealing, the free carrier density of the material recovered to approximately the same level as after the first irradiation, therefore, the low energy peaks in curves *(ii)* and *(iv)* are expected to be the same.

3.3. Laplace-DLTS analysis

We used Laplace-DLTS to investigate the peaks in the annealed sample in more detail. In Fig. 5, we have shown Laplace DLTS spectra recorded at 200 and 205 K. The spectra

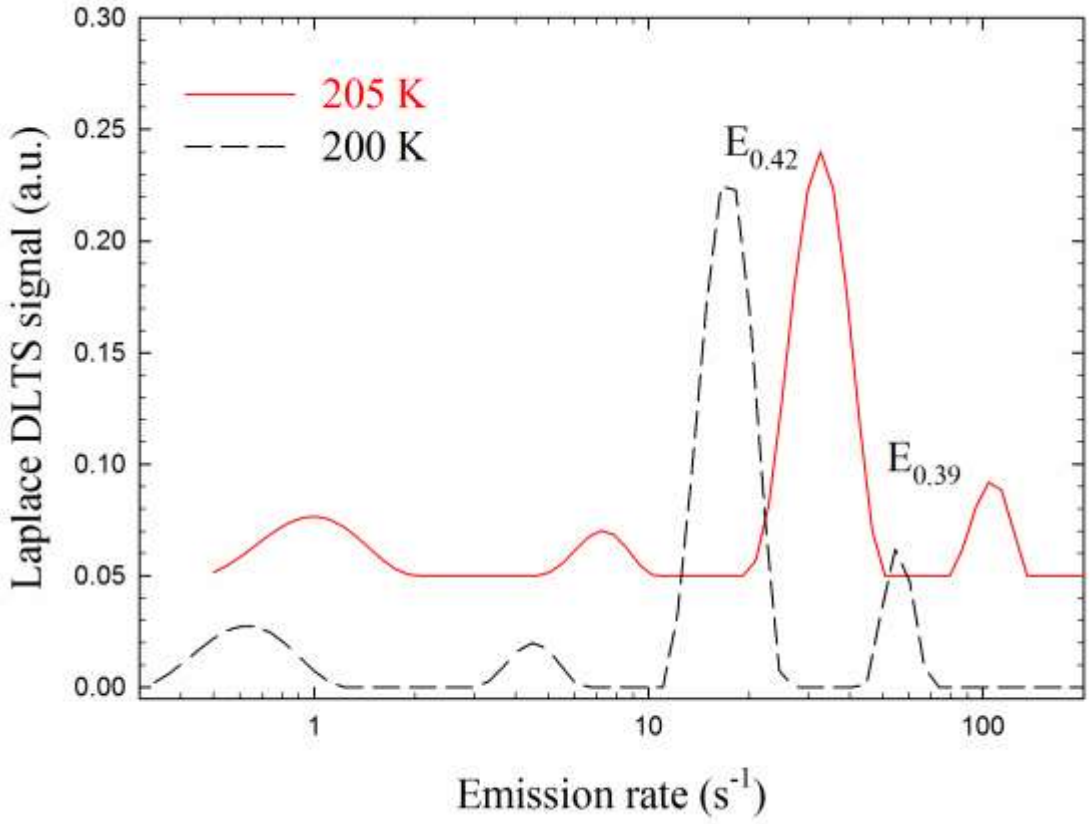

Fig. 5. Laplace-DLTS spectra recorded at different temperatures to show the presence of defects with closely spaced energy levels: (a) 200 K and 205 K.

indicate the presence of two defects, labelled $E_{0.39}$ and $E_{0.42}$ instead of the single peak observed by conventional DLTS. At 200 and 205 K, the emission rate of $E_{0.42}$ is less than one third of $E_{0.39}$. By monitoring the change of the peak positions over a wide range of temperature, it was deduced that the two small peaks appeared at lower emission rate of Fig. 5 are artefacts. The two defects are distinctly illustrated in the Arrhenius plots in Fig. 7 and their properties tabulated in Table 2.

The spectra in Fig. 6 were recorded at temperatures 300 and 310 K, and revealed the presence of peaks labelled $E_{0.65}$, $E_{0.70}$ and $E_{0.76}$. The peaks of the deep level defects were clearly separated by Laplace DLTS. The signatures of the three traps in term of activation energies were 0.65, 0.70 and 0.76 eV, and the corresponding apparent capture cross sections were 7.7×10^{-15} and 3.6×10^{-14} and 1.2×10^{-14} cm^2, respectively. The Arrhenius plots of the three defects that were successfully split by Laplace DLTS are shown in Fig. 7. The defects $E_{0.65}$ and $E_{0.70}$ are closer to each other, and have been assigned in the literature to be Z1/Z2.[20-23]. Son *et al* has recently identified the levels as the double acceptor (2–/0) of an

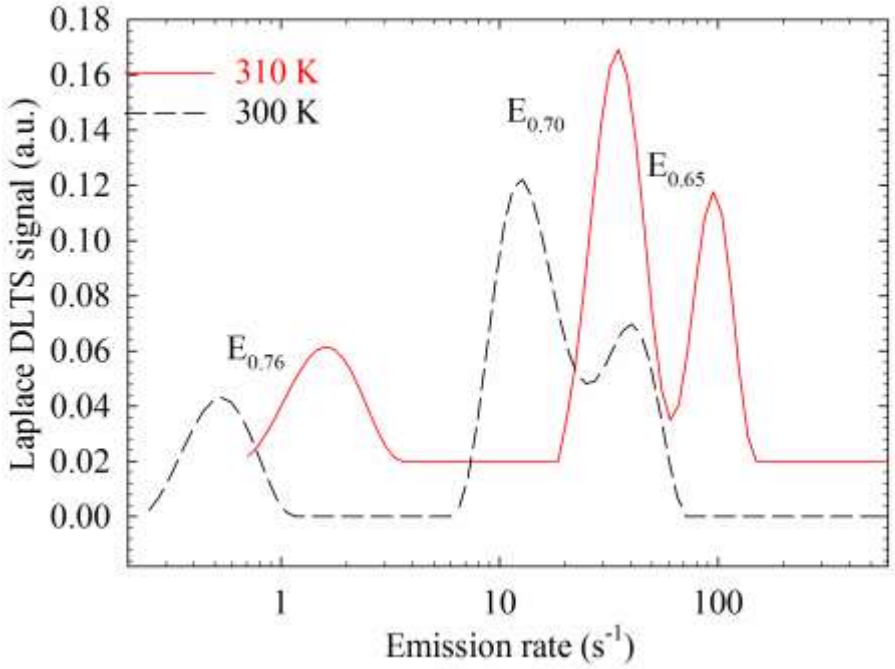

Fig. 6. Laplace-DLTS spectra recorded at different temperatures to show the presence of defects with closely spaced energy levels: (a) 300 K and 310 K, after annealing the irradiated sample, at 300 °C for 20 minutes in flowing argon.

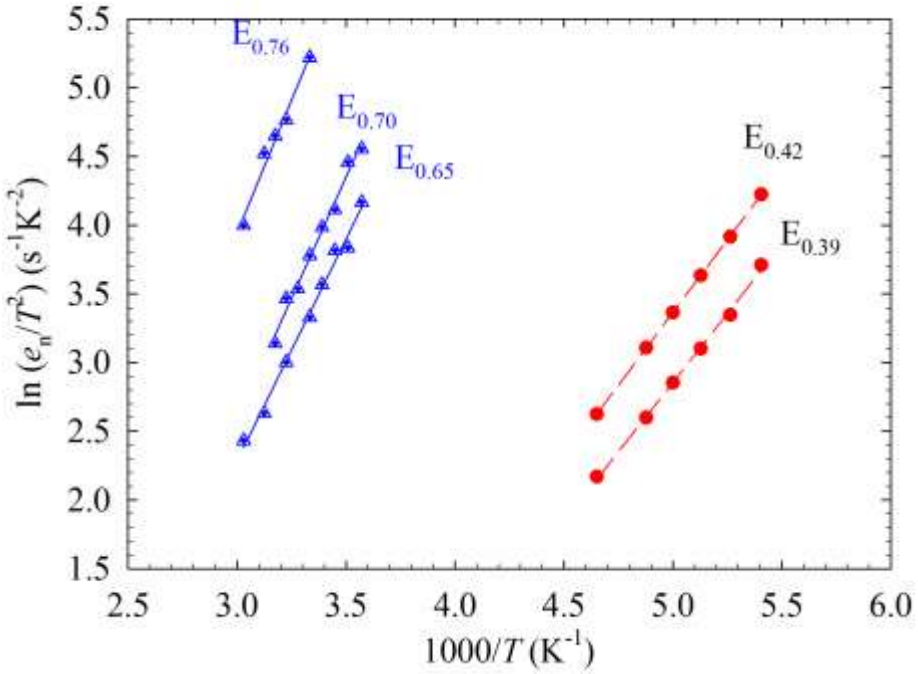

Fig. 7. Arrhenius plots of some of the deep-level defects with closely spaced energy levels, obtained after annealing the irradiated sample, at 300 °C for 20 minutes in flowing argon.

isolated carbon vacancy [23]. The defect labelled $E_{0.76}$ obtained at higher temperature side of the measurements. The structure of defect $E_{0.76}$ has not been reported despite its presence after electron and proton irradiation [19, 24].

The properties of all the defects present using both conventional and Laplace-DLTS on 4H-SiC are summarised in Table 2.

4. Conclusions

In conclusion, the results obtained from *I-V* and *C-V* characteristics at four different processes (as-grown, irradiation at fluences 4.1×10^{11} and 8.9×10^{11} cm^{-2}, annealing at 300℃) demonstrated the suitability of Ni/4H-SiC SBDs for the study. The defects introduced in *n*-type 4H-SiC during alpha-particle irradiation from a ^{241}Am radionuclide with energy of 5.4 MeV followed by annealing in flowing argon were characterised by deep level transient spectroscopy (DLTS) and high resolution Laplace-DLTS. Four deep levels with activation energies $E_{0.09}$, $E_{0.11}$, $E_{0.16}$, and $E_{0.65}$ present in as-grown material. The intensity of $E_{0.09}$ reduced to 12% after bombardment with fluences 4.1×10^{11} cm^{-2} and two new defects with trap levels $E_C - 0.39$ and $E_C - 0.62$ introduced. After the SBD received the fluence 8.9×10^{11} cm^{-2}, the shallow defect labelled ($E_{0.09}$, $E_{0.11}$ and $E_{0.16}$) disappeared. Both the lowering after the first irradiation and the disappearance of the defect may be as a result of intense damage that lowered the position of Fermi level deeper into the bandgap, thereby not filling this shallow defect during the forward bias pulse. Also, three deep levels with energy level $E_{0.55}$, $E_{0.67}$ and $E_{0.70}$ were observed. Re-appearance of shallow defects occurred after the temperature annealing of irradiated SBD at 300℃ for 20 minutes in flowing argon. Laplace-DLTS was used to split defect $E_{0.42}$ into $E_{0.39}$ and $E_{0.42}$ with the same or closely attribute related to silicon or carbon vacancy. In addition, Laplace-DLTS revealed the presence of three defects ($E_{0.65}$, $E_{0.70}$ and $E_{0.76}$), with $E_{0.65}$ and $E_{0.70}$ having close emission rates attributed to the Z_1/Z_2, which, according to literature are identified as the double acceptor of an isolated carbon vacancy. The defect labelled $E_{0.76}$ is not yet identified.

Acknowledgement

This work is based on the research supported in part by the National Research Foundation (NRF) of South African (Grant specific unique reference number (UID) 78838). The Grant holder acknowledges that opinions, findings and conclusions or recommendations expressed

in this publication generated by the NRF supported are that of authors and that NRF accepts no liability whatsoever in this regard.

References

[1] L. Pelaz, L.A. Marqués, M. Aboy, P. López, I. Santos, Eur. Phys. J. B, 72 (2009) 323-359.
[2] Ž. Pastuović, I. Capan, D.D. Cohen, J. Forneris, N. Iwamoto, T. Ohshima, R. Siegele, N. Hoshino, H. Tsuchida, Nuclear Instruments and Methods in Physics Research Section B: Beam Interactions with Materials and Atoms, 348 (2015) 233-239.
[3] A. Akbay, H. Korkut, K. Ejderha, T. Korkut, A. Türüt, Journal of Radioanalytical and Nuclear Chemistry, 289 (2011) 145-148.
[4] L.M. Tolbert, B. Ozpineci, S.K. Islam, M.S. Chinthavali, Power and Energy Systems, Proceedings, 1 (2003) 317-321.
[5] V. Kazukauskas, J.-V. Vaitkus, Opto-Electronic Review, 12 (2004) 377-382.
[6] J. Grant, W. Cunningham, A. Blue, V. O'Shea, J. Vaitkus, E. Gaubas, M. Rahman, Nuclear Instruments and Methods in Physics Research Section A: Accelerators, Spectrometers, Detectors and Associated Equipment, 546 (2005) 213-217.
[7] T. Nishijima, T. Ohshima, K.K. Lee, Nuclear Instruments and Methods in Physics Research Section B: Beam Interactions with Materials and Atoms, 190 (2002) 329-334.
[8] F. Nava, E. Vittone, P. Vanni, G. Verzellesi, P.G. Fuochi, C. Lanzieri, M. Glaser, Nuclear Instruments and Methods in Physics Research Section A: Accelerators, Spectrometers, Detectors and Associated Equipment, 505 (2003) 645-655.
[9] L. Kin Kiong, T. Ohshima, H. Itoh, Nuclear Science, IEEE Transactions on, 50 (2003) 194-200.
[10] M.C. Driver, R.H. Hopkins, C.D. Brandt, D.L. Barrett, A.A. Burk, R.C. Clarke, G.W. Eldridge, H.M. Hobgood, J.P. McHugh, P.G. McMullin, R.R. Siergiej, S. Sriram, Gallium Arsenide Integrated Circuit (GaAs IC) Symposium, 1993. Technical Digest 1993., 15th Annual, 1993, pp. 19-21.
[11] S. Yamada, B.-S. Song, T. Asano, S. Noda, Applied Physics Letters, 99 (2011) 2011021-2011023.
[12] E. Omotoso, W.E. Meyer, F.D. Auret, A.T. Paradzah, M. Diale, S.M.M. Coelho, P.J. Janse van Rensburg, Materials Science in Semiconductor Processing, 39 (2015) 112-118.
[13] T. Marinova, A. Kakanakova-Georgieva, V. Krastev, R. Kakanakov, M. Neshev, L. Kassamakova, O. Noblanc, C. Arnodo, S. Cassette, C. Brylinski, B. Pecz, G. Radnoczi, G. Vincze, Materials Science and Engineering: B, 46 (1997) 223-226.
[14] S.M. Sze, K.K. Ng, Physics of semiconductor devices, John Wiley & Sons, 2006.
[15] E. Rhoderick, R. Williams, Oxford Science, Oxford, 1988.
[16] F.D. Auret, P.N.K. Deenapanray, Critical Reviews in Solid State and Materials Sciences, 29 (2004) 1-44.
[17] E. Omotoso, W.E. Meyer, F.D. Auret, A.T. Paradzah, M. Diale, S.M.M. Coelho, P.J. Janse van Rensburg, P.N.M. Ngoepe, Nuclear Instruments and Methods in Physics Research Section B: Beam Interactions with Materials and Atoms, (2015) 5.
[18] T. Kimoto, A. Itoh, H. Matsunami, S. Sridhara, L. Clemen, R. Devaty, W. Choyke, T. Dalibor, C. Peppermüller, G. Pensl, Applied physics letters, 67 (1995) 2833-2835.
[19] J. Doyle, M.K. Linnarsson, P. Pellegrino, N. Keskitalo, B. Svensson, A. Schoner, N. Nordell, J. Lindstrom, Journal of applied physics, 84 (1998) 1354-1357.
[20] T. Dalibor, G. Pensl, H. Matsunami, T. Kimoto, W.J. Choyke, A. Schöner, N. Nordell, physica status solidi (a), 162 (1997) 199-225.
[21] C. Hemmingsson, N.T. Son, O. Kordina, J.P. Bergman, E. Janzén, J.L. Lindström, S. Savage, N. Nordell, Journal of Applied Physics, 81 (1997) 6155-6159.
[22] I. Pintilie, L. Pintilie, K. Irmscher, B. Thomas, Applied Physics Letters, 81 (2002) 4841-4843.
[23] N.T. Son, X.T. Trinh, L.S. Løvlie, B.G. Svensson, K. Kawahara, J. Suda, T. Kimoto, T. Umeda, J. Isoya, T. Makino, T. Ohshima, E. Janzén, Physical Review Letters, 109 (2012) 187603.
[24] A. Castaldini, A. Cavallini, L. Rigutti, F. Nava, Applied Physics Letters, 85 (2004) 3780-3782.
[25] A.A. Lebedev, Semiconductors, 33 (1999) 107-130.